SYNTHESIS AND CHARACTERIZATION OF HIGH DIELECTRIC CONSTANT MATERIAL BASED ON Er- DOPED $BaTiO_3$ FOR CAPACITOR APPLICATIONS

by

FATIN ADILA BINTI ISMAIL
(1630312166)

A thesis submitted in fulfillment of the requirements for the degree of Master of Science in Electronic Engineering

School of Microelectronic Engineering
UNIVERSITI MALAYSIA PERLIS

2018

UNIVERSITI MALAYSIA PERLIS

DECLARATION OF THESIS

Author's Full Name : FATIN ADILA BINTI ISMAIL

Title : SYNTHESIS AND CHARACTERIZATION OF HIGH DIELECTRIC CONSTANT MATERIAL BASED ON Er-DOPED $BaTiO_3$ FOR CAPACITOR APPLICATIONS

Date of Birth : 16 FEBRUARY 1992

Academic Session : 2016/2017

I hereby declare that this thesis becomes the property of Universiti Malaysia Perlis (UniMAP) and to be placed at the library of UniMAP. This thesis is classified as:

☐ **CONFIDENTIAL** (Contains confidential information under the Official Secret Act 1997)*

☐ **RESTRICTED** (Contains restricted information as specified by the organization where research was done)*

☑ **OPEN ACCESS** I agree that my thesis to be published as online open access (Full Text)

I, the author, give permission to reproduce this thesis in whole or in part for the purpose of research or academic exchange only (except during the period of _____ years, if so requested above)

Certified by:

SIGNATURE	**SIGNATURE OF SUPERVISOR**
920216036064	DR. ROZANA AINA MAULAT OSMAN
(NEW IC NO. /PASSPORT NO.)	**NAME OF SUPERVISOR**

© This item is protected by original copyright

NOTES : * If the thesis is CONFIDENTIAL or RESTRICTED, please attach with the letter from the organization with the period and reasons for confidentiality or restriction. Replace thesis with dissertation (MSc by Mixed Mode) or with report (coursework)

ACKNOWLEDGMENT

In the name of Allah, Most Gracious, Most Merciful.

First and foremost I want to thank my advisor Dr. Rozana Aina Maulat Osman for her teaching, guidance, encouragement and patience during my graduate studies in University Malaysia Perlis. Further, it has been an honor to work with her as a MSc. student and her enthusiasm for research was courageous and motivated me even at the hardship of the MSc. pursuit.

I also want to thank Dr. Sobri Idris for his support and valuable suggestions through this study. Further, I take this opportunity to thank him for his commitment for my excellence. My gratitude is also extended to lecturers and technicians of School of Microelectronic Engineering and School of Materials Engineering, UniMAP, for helping me analyzing the samples and the input given.

The members of my group, Qing, Masku, Dhaniah, Najwa, Farah, Hamidah, Amirah, Fashren, Yuk Ming and Soo Soo Peng are also kindly acknowledged. Their contribution to my research as well as my personal life was immense.

This work is supported by the Ministry of High Education (MOHE) under Fundamental Research Grants Scheme (FRGS), which support is gratefully acknowledged. Besides, the scholarship from MyMaster also gives a big help.

Finally, I would also give my special appreciation to my family members for their unconditional love and support my entire life and brought me up to this level. Last but not least, thank you to all the people around me who involved in this research neither directly nor indirectly.

©This item is protected by original copyright

TABLE OF CONTENTS

		PAGE
DECLARATION OF THESIS		**ii**
ACKNOWLEDGMENT		**iii**
TABLE OF CONTENTS		**iv**
LIST OF TABLES		**viii**
LIST OF FIGURES		**x**
LIST OF ABBREVIATIONS		**xiv**
LIST OF SYMBOLS		**xvi**
ABSTRAK		**xix**
ABSTRACT		**xx**
CHAPTER 1 : INTRODUCTION		**1**
1.1	Background	1
1.2	Basic structure of capacitor	2
1.3	Properties of dielectric material in capacitor	3
1.4	Problem statement	6
1.5	Objectives	8
1.6	Scope of study	8
1.7	Thesis structure	9
CHAPTER 2 : LITERATURE REVIEW		**11**
2.1	Introduction	11
2.2	Dielectric material	12
	2.2.1 Dielectric constant	13
	2.2.2 Dielectric loss	14

©This item is protected by original copyright

2.2.3 Dielectric strength 14

2.3 History of Barium titanate ($BaTiO_3$) 15

2.3.1 Perovskite structure of $BaTiO_3$ 15

2.3.2 Phase transition of $BaTiO_3$ 18

2.3.3 Electrical properties of $BaTiO_3$ 19

2.3.3.1 Dielectric 19

2.3.3.2 Ferroelectricity 23

2.3.3.3 Piezoelectricity 24

2.3.3.4 Pyroelectricity 24

2.3.4 Microstructural properties of $BaTiO_3$ 25

2.4 Doped-$BaTiO_3$ 26

2.5 Er-doped $BaTiO_3$ 28

CHAPTER 3 : METHODOLOGY **31**

3.1 Introduction 31

3.2 Material used for synthesis of $BaTiO_3$ and Er-doped $BaTiO_3$ 31

3.3 Synthesis of $BaTiO_3$ and Er-doped $BaTiO_3$ 32

3.4 Characterization of $BaTiO_3$ and Er-doped $BaTiO_3$ 35

3.4.1 X-ray Diffraction (XRD) 35

3.4.2 Rietveld refinement analysis 39

3.4.3 Impedance analyser 41

3.4.4 Scanning Electron Microscopy (SEM) 43

CHAPTER 4 : RESULT & DISCUSSION **45**

4.1 Introduction 45

4.2 Structural analysis 45

4.2.1 XRD analysis of $BaTiO_3$ 45

©This item is protected by original copyright

4.2.2 XRD analysis of composition $Ba_{1-x}Er_xTiO_3$ for ($0 \leq x \leq 0.05$) 47

4.2.3 Lattice parameters of composition $Ba_{1-x}Er_xTiO_3$ for ($0 \leq x \leq 0.05$) 49

4.2.4 Crystallite size of composition $Ba_{1-x}Er_xTiO_3$ for ($0 \leq x \leq 0.01$) 52

4.3 Rietveld refinement analysis 53

4.3.1 Initial structure model for $BaTiO_3$ 53

4.3.2 Rietveld refinement of $Ba_{1-x}Er_xTiO_3$ for x=0.0025, 0.005, 0.0075 and 0.01 68

4.3.2.1 Assumption if Er located at A-site 70

4.3.2.2 Assumption if Er located at B-site 79

4.3.2.3 Summary of Er-doped $BaTiO_3$ in $Ba_{1-x}Er_xTiO_3$ for ($0 \leq x \leq 0.01$) 88

4.4 Microstructural analysis of $Ba_{1-x}Er_xTiO_3$ for ($0 \leq x \leq 0.01$) 91

4.5 Electrical analysis 94

4.5.1 Electrical properties for $BaTiO_3$ 94

4.5.2 Electrical properties of $Ba_{1-x}Er_xTiO_3$ for ($0 \leq x \leq 0.01$) 101

4.5.2.1 Dielectric constant 101

4.5.2.2 Curie-Weiss plot 105

4.5.2.3 Capacitance 107

4.5.2.4 Dielectric loss 111

4.5.2.5 Conductivity 113

4.5.3 Capacitance-Voltage characteristic of $Ba_{1-x}Er_xTiO_3$ for ($0 \leq x \leq 0.01$) 116

CHAPTER 5 : CONCLUSION **118**

5.1 Introduction 118

5.2 Recommendation for future work 120

©This item is protected by original copyright

5.3 Commercialisation potential 120

REFERENCES **121**

APPENDIX A **126**

APPENDIX B **127**

LIST OF PUBLICATIONS **131**

©This item is protected by original copyright

LIST OF TABLES

NO.		PAGE
Table 2.1:	Examples of dielectric materials with their dielectric constant (Wilk, Wallace, & Anthony, 2001; Ye, 2008)	13
Table 2.2:	Tolerance factor value with respective crystal structure (Harry & Yakel, 1965).	17
Table 2.3:	Capacitance value and their possible phenomena (Sinclair, 1995).	23
Table 2.4:	Conductivity value for related class of materials (A. R. West, 2014).	23
Table 2.5:	Dielectric constant of rare earth-doped $BaTiO_3$ at T_C.	27
Table 3.1:	List of materials used in synthesis of $BaTiO_3$ and Er-doped $BaTiO_3$	31
Table 3.2:	Drying temperature of raw materials	32
Table 3.3:	Example of intial structure model of $BaTiO_3$	39
Table 4.1:	Lattice parameters and unit cell volume for $Ba_{1-x}Er_xTiO_3$ for ($0 \leq x \leq 0.05$).	50
Table 4.2:	Crystallite size for composition $Ba_{1-x}Er_xTiO_3$ ($0 \leq x \leq 0.01$).	53
Table 4.3:	Starting structural model for $BaTiO_3$ (Model A).	55
Table 4.4:	Starting structural model for $BaTiO_3$ (Model B).	55
Table 4.5:	Starting structural model for $BaTiO_3$ (Model C).	55
Table 4.6:	Starting structural model for $BaTiO_3$ (Model D).	56
Table 4.7:	Starting structural model for $BaTiO_3$ (Model E).	56
Table 4.8:	Structural data for $BaTiO_3$ powder synthesised at 1400°C for 12 hours obtained from Rietveld refinement by using Model A.	59
Table 4.9:	Structural data for $BaTiO_3$ powder synthesised at 1400°C for 12 hours obtained from Rietveld refinement by using Model B.	60
Table 4.10:	Structural data for $BaTiO_3$ powder synthesised at 1400°C for 12 hours obtained from Rietveld refinement by using Model C.	61
Table 4.11:	Structural data for $BaTiO_3$ powder synthesised at 1400°C for 12 hours obtained from Rietveld refinement by using Model D.	62

©This item is protected by original copyright

Table 4.12: Structural data for $BaTiO_3$ powder synthesised at 1400°C for 12 hours obtained from Rietveld refinement by using Model E. 63

Table 4.13: Refined structural data for Model A, Model C and Model D. 68

Table 4.14: Structural data for Er-doped $BaTiO_3$ powder synthesised at 1400°C obtained from Rietveld refinement (x=0.0025). 70

Table 4.15: Structural data for Er-doped $BaTiO_3$ powder synthesised at 1400°C obtained from Rietveld refinement (x=0.005). 71

Table 4.16: Structural data for Er-doped BaTiO3 powder synthesised at 1400°C obtained from Rietveld refinement (x=0.0075). 72

Table 4.17: Structural data for Er-doped $BaTiO_3$ powder synthesised at 1400°C obtained from Rietveld refinement (x=0.01). 73

Table 4.18: Structural data for Er-doped $BaTiO_3$ powder synthesised at 1400°C obtained from Rietveld refinement (x=0.0025). 79

Table 4.19: Structural data for Er-doped $BaTiO_3$ powder synthesised at 1400°C obtained from Rietveld refinement (x=0.005). 80

Table 4.20: Structural data for Er-doped BaTiO3 powder synthesised at 1400°C obtained from Rietveld refinement (x=0.0075). 81

Table 4.21: Structural data for Er-doped $BaTiO_3$ powder synthesised at 1400°C obtained from Rietveld refinement (x=0.01). 82

Table 4.22: Refined structural data for the possibility of Er-doped $BaTiO_3$ were located at A-site. 89

Table 4.23: Refined structural data for the possibility of Er-doped $BaTiO_3$ were located at B-site. 90

©This item is protected by original copyright

LIST OF FIGURES

NO.		PAGE
Figure 1.1:	A typical capacitor and its basic structure (Callister, 2001; Tournier, 2014) .	2
Figure 1.2:	Parallel plate capacitor (a) without and (b) with dielectric material between the plates.	3
Figure 1.3:	Production of multilayer capacitor in ten years (Kishi et al., 2003).	6
Figure 2.1:	The ideal ABO_3 perovskite structure (Pradhan & Roy, 2013).	16
Figure 2.2:	The structure changes of $BaTiO_3$ (Heywang, W., Lubitz, K. and Wersing, 2009).	18
Figure 2.3:	Temperature dependence of permittivity for $BaTiO_3$ (A. R. West, 2014).	20
Figure 2.4:	Curie-Weiss plot (A. R. West, 2014).	21
Figure 2.5:	Variation of dielectric constant vs frequency (A. J. Moulson & Herbert, 2003).	22
Figure 2.6:	Room temperature X-ray diffraction patterns of (a) $BaTiO_3$ and (b) $Ba_{0.99}Er_{0.01}TiO_3$ (Leyet et al., 2012).	29
Figure 2.7:	Temperature dependence of the real and imaginary parts of the dielectric constant of (a) $BaTiO_3$ and (b) $Ba_{0.99}Er_{0.01}TiO_3$ ceramics measured at 1 MHz (Leyet et al., 2012)	30
Figure 2.8:	Frequency dependence of the AC conductivity of $Ba_{0.99}Er_{0.01}TiO_3$ ceramic samples measured at different temperatures (Leyet et al., 2012).	30
Figure 3.1:	Flowchart of process involve in synthesized and characterized of $BaTiO_3$ and $Ba_{1-x}Er_xTiO_3$	34
Figure 3.2:	Example of PDF of a XRD pattern (PDF 00-005-0626)	36
Figure 3.3:	Magnified image of data in PDF card (PDF 00-005-0626)	36
Figure 3.4:	(a) Equipment used in preparation of samples for XRD; (b) sample preparation for XRD analysis; (c) flat surface sample prepared for XRD and (d) XRD process of the sample	37
Figure 3.5:	Conventional jig for impedance measurement.	43
Figure 4.1:	XRD pattern of $BaTiO_3$ compared with PDF card [00-005-0626].	46

©This item is protected by original copyright

Figure 4.2: XRD pattern of $Ba_{1-x}Er_xTiO_3$ for ($0 \leq x \leq 0.05$). 48

Figure 4.3: XRD pattern of $Ba_{1-x}Er_xTiO_3$ at x=0.02 and x=0.05 compared with PDF card [00-054-0181] of $Er_2Ti_2O_7$ impurities 49

Figure 4.4: Lattice *a* for $Ba_{1-x}Er_xTiO_3$ for ($0 \leq x \leq 0.01$) as a function of *x*. 51

Figure 4.5: Lattice *c* for $Ba_{1-x}Er_xTiO_3$ for ($0 \leq x \leq 0.01$) as a function of *x*. 51

Figure 4.6: Unit cell volume for $Ba_{1-x}Er_xTiO_3$ for ($0 \leq x \leq 0.01$) as a function of *x*. 52

Figure 4.7: Rietveld plots for undoped $BaTiO_3$ (Model A). 64

Figure 4.8: Rietveld plots for undoped BaTiO3 (Model B). 65

Figure 4.9: Rietveld plots for undoped $BaTiO_3$ (Model C). 65

Figure 4.10: Rietveld plots for undoped $BaTiO_3$ (Model D). 66

Figure 4.11: Rietveld plots for undoped $BaTiO_3$ (Model E). 66

Figure 4.12: Comparison of R-values and χ^2 for all models. 67

Figure 4.13: Rietveld refinement of $Ba_{1-x}Er_xTiO_3$ for x=0.0025. 74

Figure 4.14: Rietveld refinement of $Ba_{1-x}Er_xTiO_3$ for x=0.005. 75

Figure 4.15: Rietveld refinement of $Ba_{1-x}Er_xTiO_3$ for x=0.0075 75

Figure 4.16: Rietveld refinement of $Ba_{1-x}Er_xTiO_3$ for x=0.01. 76

Figure 4.17: The goodness-of-fit, χ^2 and R-factors vs x in $Ba_{1-x}Er_xTiO_3$. 76

Figure 4.18: Lattice *a* for $Ba_{1-x}Er_xTiO_3$ for ($0 \leq x \leq 0.01$) as a function of *x*. 77

Figure 4.19: Lattice *c* for $Ba_{1-x}Er_xTiO_3$ for ($0 \leq x \leq 0.01$) as a function of *x*. 78

Figure 4.20: Unit cell volume for $Ba_{1-x}Er_xTiO_3$ for ($0 \leq x \leq 0.01$) as a function of *x*. 78

Figure 4.21: Rietveld refinement of $Ba_{1-x}Er_xTiO_3$ for x=0.0025**.** 83

Figure 4.22: Rietveld refinement of $Ba_{1-x}Er_xTiO_3$ for x=0.005. 84

Figure 4.23: Rietveld refinement of $Ba_{1-x}Er_xTiO_3$ for x=0.0075. 84

Figure 4.24: Rietveld refinement of $Ba_{1-x}Er_xTiO_3$ for x=0.01. 85

Figure 4.25: The goodness-of-fit, χ^2 and R-factors vs x in $Ba_{1-x}Er_xTiO_3$. 85

Figure 4.26: Lattice *a* for $Ba_{1-x}Er_xTiO_3$ for ($0 \leq x \leq 0.01$) as a function of *x*. 86

©This item is protected by original copyright

Figure 4.27: Lattice *c* for $Ba_{1-x}Er_xTiO_3$ for ($0 \leq x \leq 0.01$) as a function of *x*. 87

Figure 4.28: Unit cell volume for $Ba_{1-x}Er_xTiO_3$ for ($0 \leq x \leq 0.01$) as a function of *x*. 87

Figure 4.29: Scanning electron micrographs of sintered $Ba_{1-x}Er_xTiO_3$ for ($0 \leq x \leq 0.01$). 92

Figure 4.30: Grain size distribution of sintered $Ba_{1-x}Er_xTiO_3$ for ($0 \leq x \leq 0.01$). 93

Figure 4.31: Dielectric constant of $BaTiO_3$ as a function of temperatures at different frequencies. 95

Figure 4.32: Curie-Weiss plot of $BaTiO_3$ at different frequency as a function of temperatures. 96

Figure 4.33: Capacitance of $BaTiO_3$ at different temperature as a function of frequency. 97

Figure 4.34: Capacitance of $BaTiO_3$ at 30˚C, 110˚C (T_C) and 200˚C as a function of frequency. 98

Figure 4.35: Dielectric loss (Tan δ) of $BaTiO_3$ at different temperature as a function of frequency. 99

Figure 4.36: Conductivity of $BaTiO_3$ at different temperature as a function of frequency. 100

Figure 4.37: Conductivity of $BaTiO_3$ at 30˚C, 110˚C (T_C) and 200˚C as a function of frequency. 101

Figure 4.38: Dielectric constant of $Ba_{1-x}Er_xTiO_3$ for ($0 \leq x \leq 0.01$) as a function of temperature at 1 kHz. 103

Figure 4.39: Dielectric constant of $Ba_{1-x}Er_xTiO_3$ for ($0 \leq x \leq 0.01$) as a function of temperature at 10 kHz. 104

Figure 4.40: Dielectric constant of $Ba_{1-x}Er_xTiO_3$ for ($0 \leq x \leq 0.01$) as a function of temperature at 100 kHz. 104

Figure 4.41: Curie-Weiss plot of $Ba_{0.9975}Er_{0.0025}TiO_3$ at different frequency as a function of temperature. 105

Figure 4.42: Curie-Weiss plot of $Ba_{0.995}Er_{0.005}TiO_3$ at different frequency as a function of temperature. 106

Figure 4.43: Curie-Weiss plot of $Ba_{0.9925}Er_{0.0075}TiO_3$ at different frequency as a function of temperature. 106

Figure 4.44: Curie-Weiss plot of $Ba_{0.99}Er_{0.01}TiO_3$ at different frequency as a function of temperature. 107

©This item is protected by original copyright

Figure 4.45: Capacitance of $Ba_{0.9975}Er_{0.0025}TiO_3$ at 30˚C, 120˚C (T_C) and 200˚C as a function of frequency. 109

Figure 4.46: Capacitance of $Ba_{0.995}Er_{0.005}TiO_3$ at 30˚C, 120˚C (T_C) and 200˚C as a function of frequency. 109

Figure 4.47: Capacitance of $Ba_{0.9925}Er_{0.0075}TiO_3$ at 30˚C, 120˚C (T_C) and 200˚C as a function of frequency. 110

Figure 4.48: Capacitance of $Ba_{0.99}Er_{0.01}TiO_3$ at 30˚C, 120˚C (T_C) and 200˚C as a function of frequency. 110

Figure 4.49: Dielectric loss (Tan δ) of $Ba_{1-x}Er_xTiO_3$ for ($0 \leq x \leq 0.01$) as a function of temperature at 1kHz. 111

Figure 4.50: Dielectric loss (Tan δ) of $Ba_{1-x}Er_xTiO_3$ for ($0 \leq x \leq 0.01$) as a function of temperature at 10kHz. 112

Figure 4.51: Dielectric loss (Tan δ) of $Ba_{1-x}Er_xTiO_3$ for ($0 \leq x \leq 0.01$) as a function of temperature at 100kHz. 112

Figure 4.52: Conductivity of $Ba_{0.9975}Er_{0.0025}TiO_3$ at 30˚C, 120˚C (T_C) and 200˚C as a function of frequency. 114

Figure 4.53: Conductivity of $Ba_{0.995}Er_{0.005}TiO_3$ at 30˚C, 120˚C (T_C) and 200˚C as a function of frequency. 114

Figure 4.54: Conductivity of $Ba_{0.9925}Er_{0.0075}TiO_3$ at 30˚C, 120˚C (T_C) and 200˚C as a function of frequency. 115

Figure 4.55: Conductivity of $Ba_{0.99}Er_{0.01}TiO_3$ at 30˚C, 120˚C (T_C) and 200˚C as a function of frequency. 115

Figure 4.56: Capacitance-Voltage characteristic of $Ba_{1-x}Er_xTiO_3$ ($0 \leq x \leq 0.01$) at 100kHz. 117

©This item is protected by original copyright

LIST OF ABBREVIATIONS

$BaCO_3$	Barium carbonate
$BaTiO_3$	Barium titanate
$CaTiO_3$	Calcium titanate
Ce	Cerium
Dy	Dysprosium
Er	Erbium
Er_2O_3	Erbium oxide
FWHM	Full width half maximum
Gd	Gadolinium
H_2O	Water
HCL	Hydrochloric acid
HF	Hydrofluoric acid
Ho	Holmium
Hz	Hertz
ICDD	International Centre of Diffraction Data
ICSD	International Crystal Structure Database
kHz	Kilohertz
$KNbO_3$	Potassium niobate
La	Lanthanum
Lu	Lutetium
$MgTiO_3$	Magnesium titanate
MHz	Megahertz
MLCC	Multilayer ceramic capacitor

©This item is protected by original copyright

Nd	Neodymium
$PbTiO_3$	Lead titanate
PDF	Powder diffraction file
PLZT	Lead lanthanum zirconate titanate
Pm	Promethium
Pr	Praseodymium
PTC	Positive Temperature Coefficient
PZT	Lead zirconate titanate
SEM	Scanning Electron Microscope
SiO_2	Silicon dioxide
Sm	Samarium
Eu	Europium
Tb	Terbium
Ti	Titanium
TiO_2	Titanium dioxide
TiO_2	Titanium dioxide
Tm	Thulium
XRD	X-Ray Diffraction
Y	Yttrium
Yb	Ytterbium

©This item is protected by original copyright

LIST OF SYMBOLS

C	Capacitance
Q	Charge
V	Applied voltage
ε_o	Dielectric constant of free space
F	Farad
m	Meter
A	Area
t	Thickness of plates
k	Dielectric constant
ε_r	Relative permittivity
Tan δ	Dielectric loss
Pm3m	Space group
Ba^{2+}	Barium ion
Ti^{4+}	Titanium ion
t	Tolerance factor
r_A	Ionic radii of A
r_B	Ionic radii of B
r_O	Ionic radii of O
La^{3+}	Lanthanum ion
Nd^{3+}	Neodymium ion
Tm^{3+}	Thulium ion
Lu^{3+}	Lutetium
Er^{3+}	Erbium ion

©This item is protected by original copyright

Y^{3+}	Yttrium ion
T_c	Curie temperature
Pm-3m	Space group
P4mm	Space group
C2mm	Space group
Rm3	Space group
C_p	Parallel capacitance
σ	Conductivity
˚C	Degree celcius
C	Curie constant
T	Temperature of sample in Kelvin
θ	Curie Weiss temperature
cm	Centimeter
S	Siemens
μ	Micro
Nd^{3+}	Nd 3+ ion
Dy^{3+}	Dy 3+ ion
Min	Minutes
2θ	2 Theta
˚	Degree
n	Integer (n=1,2,…)
λ	Lambda
d_{hkl}	Interplanar spacing
D	Crystallite size
K	Shape factor

©This item is protected by original copyright

β	Peak width
θ	Bragg's angle
U_{iso}	Thermal parameter
Å	Armstrong
R_P	Parallel resitance
ρ	Resistivity
Ω	Ohm
mL	Millimeter

©This item is protected by original copyright

Sintesis dan Pencirian Bahan Pemalar Dielektrik yang Tinggi Berdasarkan Er-doped $BaTiO_3$ untuk Aplikasi Kapasitor

ABSTRAK

Hala pengecilan dalam teknologi peranti pintar dan alat elektronik telah menjadikan bahan yang mempunyai pemalar dielektrik yang tinggi menjadi satu parameter yang penting untuk digunakan sebagai kapasitor bagi penyimpanan data dalam alatan elektronik. Dalam kajian ini, $BaTiO_3$ telah digunakan kerana ia dilaporkan mempunyai pemalar dielektrik yang tinggi (ε_r= 4000-10000) pada suhu Curie (T_C) dalam lingkungan 110˚C. Tambahan pula, Erbium (Er) telah dilaporkan bahawa sekiranya Er digantikan (didopkan) ke dalam $BaTiO_3$, ia dapat meningkatkan sifat dielektrik $BaTiO_3$. Komposisi $BaTiO_3$ dan $BaTiO_3$ didopkan Er dalam kadar ($0 \leq x \leq 0.01$) telah disediakan melalui kaedah sintesis keadaan pepejal. Pencirian komposisi-komposisi ini telah dilakukan dengan menggunakan Belauan sinar-X (XRD), Mikroskop Imbasan Elektron (SEM) dan Analisis Impedans. Analisi XRD menunjukkan bahawa $BaTiO_3$ dan $BaTiO_3$ didopkan Er telah mencapai fasa tunggal selepas dibakar pada suhu 1400˚C. Kedua-dua $BaTiO_3$ dan $BaTiO_3$ didopkan Er mempunyai struktur tetragonal dengan kumpulan ruang P4mm. Had maksimum bagi $BaTiO_3$ didopkan Er ialah melebihi x=0.01. Untuk analisis struktur, analisis pembaikkan Rietveld telah dilakukan untuk 5 model $BaTiO_3$ (A,B,C,D and E) bagi mencari model yang mempunyai posisi atom yang sesuai serta mempunyai nilai χ^2 yang rendah dan ia akan digunakan sebagai model asas untuk pembaikkan sampel $BaTiO_3$ didopkan Er yang lain. Model C merupakan model terbaik yang mempunyai nilai χ^2 yang rendah dalam linkungan 3.808. Melalui analisi pembaikkan Rietveld, kita akan menyelidik mengenai penggantian Er ke dalam bahagian A dan B dalam struktur perovskite ABO_3. Hasilnya, Er boleh digantikan ke dalam kedua-dua bahagian A dan B kerana mempunyai nilai χ^2 yang hampir sama. Untuk analisis mikrostruktur, SEM telah digunakan untuk mengkaji kesan saiz bijian ke atas $BaTiO_3$ apabila ia digantikan dengan Er. Saiz bijian yang paling kecil untuk $Ba_{1-x}Er_xTiO_3$ adalah 3.76 μm pada x=0.0075. Untuk sifat elektrikal, komposisi $Ba_{1-x}Er_xTiO_3$ pada x=0.0075 mempunyai nilai pemalar dielektrik yang tertinggi, ε_r= ~ 6500 dibandingkan dengan $BaTiO_3$ yang mempunyai nilai pemalar dielektrik, ε_r= ~ 5200. Selain itu, sampel pada x=0.0075 mempunyai nilai kehilangan dielektrik yang rendah daripda 0.1. Nilai kemuatan yang tertinggi pada x=0.0075 iaitu pada nilai pemalar dielektrik yang tertinggi ialah C= ~4 x 10^{-9} Fcm^{-1} dengan jumlah konduktiviti, σ= 4 x $10^{-7}$$Scm^{-1}$. Sifat Kemuatan-Voltan (C-V) juga dinilai dari 0 sehingga 30 V dan kesemua sampel mempunyai kemuatan yang tinggi setelah voltan meningkat sehingga 30 V tanpa tanda kerosakkan. Sampel yang mempunyai pemalar dielektrik yang tertinggi, kadar kehilangan dielektrik yang rendah dan sifat C-V yang bagus adalah sampel pada x= 0.0075.

© This item is protected by original copyright

Synthesis and Characterization of High Dielectric Constant Material Based on Er-doped $BaTiO_3$ for Capacitor Application

ABSTRACT

High dielectric constant material becomes an important parameter to be used as capacitor for storage in most electronic devices due to miniaturization trend of smart devices and electronic gadgets. $BaTiO_3$ was used in this study as it was reported to have a high dielectric constant (ε_r= 4000-10000) at Curie temperature (T_C) around 110˚C. Furthermore, it was reported that by doping Erbium (Er) into $BaTiO_3$, it can improve the dielectric properties of $BaTiO_3$. $BaTiO_3$ and Er-doped $BaTiO_3$ with composition of $Ba_{1-x}Er_xTiO_3$ in the range of ($0 \leq x \leq 0.01$) have been synthesized via conventional solid state reaction method. The characterizations of these compositions were made using X-ray Diffraction (XRD), Scanning Electron Microscopy (SEM) analysis and Impedance Analyzer analysis. XRD analysis shows that $BaTiO_3$ and Er-doped $BaTiO_3$ has phase pure after heating at 1400˚C. Both $BaTiO_3$ and Er-doped $BaTiO_3$ exhibit tetragonal structure with space group of P4mm. Solid solution limit of Er-doped $BaTiO_3$ composition is beyond x=0.01. For structural analysis, Rietveld refinement analysis were done on $BaTiO_3$ for 5 models (A, B, C, D and E) to find the suitable atomic position with low χ^2 value to be used as standard model to refine other Er-doped $BaTiO_3$ samples. Model C is the best model with low χ^2 value of 3.808. With Rietveld refinement analysis, study on incorporation of Er into the A-site and B-site of perovskite ABO_3 structure was done. The result indicates that Er can be at both side either A or B site because of the χ^2 value that is very similar. For microstructural analysis, SEM was used to study the grain size effect by doping Er into $BaTiO_3$. The smallest grain size for $Ba_{1-x}Er_xTiO_3$ was 3.76 μm at x=0.0075. For electrical properties, the composition of $Ba_{1-x}Er_xTiO_3$ at x=0.0075 has the highest dielectric constant value, ε_r= ~ 6500 as compared to pure $BaTiO_3$ with dielectric constant value, ε_r= ~ 5200. Instead of that, the sample at x=0.0075 has low dielectric loss with value less than 0.1. The highest capacitance value for x=0.0075 at the highest dielectric constant value is C= ~4 x 10^{-9} Fcm^{-1} with total conductivity, σ= 4 x 10^{-7} Scm^{-1}. The Capacitance-Voltage (C-V) characteristic were measured from 0 to 30 V and all the samples show a high capacitance by increasing the voltage up to 30 V with no signal of breakdown region. The sample with the highest dielectric constant, low loss and good C-V characteristic is the sample with x= 0.0075.

©This item is protected by original copyright

CHAPTER 1 : INTRODUCTION

1.1 Background

Energy storage is very important in many fields as it can improve the quality of life. It is constantly driven by technological challenges and innovation. It provides the basic components to support a variety of electronic devices including computers, industrial controls, consumer automotive devices, and digital switches. One of the commonly used components in this field is capacitor. Capacitor is an important electronic component that is widely used in electronic industry to store electrical charges. There are many types of capacitor such as ceramic capacitors, film capacitors, electrolytic capacitors and supercapacitors. The capacitors might have different types but all of them have the same function which is storing energy (Ekanath, 2012; Hao, 2013)

In current technology, miniaturization is the trend to produce smaller electronic product and devices. As an example, the evolution of computer from giant-size computer to the netbook that is more smaller with improve functions. Consequently, in modern electronics industry, people attempts to reduce the size of the electronic devices to be small and light as possible. Thus, the electronic devices are driven by miniaturization. The devices will have reduction in size with the same function without compromising the performance and the reliability of devices. One of the best possible ways to achieve component size reduction is through the improvement of component in devices. Capacitors are energy storage devices used in most of the modern electronic

©This item is protected by original copyright

applications. Multilayer ceramic capacitor (MLCC) is the most widely used in microelectronic devices, made of titanate based materials. Most of it constitutes more than half of the entire global capacitor market, worth multibillion U.S dollars. Most of MLCC used in application such as mobile electronic equipment (cellular phones or portable personal computers). The use of MLCC's dominate at present and will play a major role in future (Kishi, Mizuno, & Chazono, 2003; Sakabe, 1997; Wu, Wang, & Zeng, 2012).

©This item is protected by original copyright

1.2 Basic structure of capacitor

Many different kinds of capacitors are available in the market, comprising very small capacitor beads used in resonance circuits to large power factor correction capacitors. Capacitors are basically formed with the same basic structure which consists of two parallel conductive (metal) plates which are not connected with each other, but electrically separated either by vacuum or by some form of a good insulating material such as waxed paper, mica, ceramic, plastic or some form of a liquid gel as used in electrolytic capacitors as shown in Figure 1.1. The insulating layer between the capacitor plates is commonly called the dielectric (Callister, 2001; Tournier, 2014).

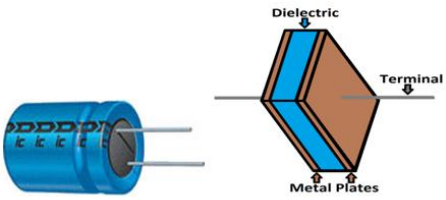

Figure 1.1: A typical capacitor and its basic structure (Callister, 2001; Tournier, 2014)

.

1.3 Properties of dielectric material in capacitor

Ideally, dielectric properties can be defined from the behaviour of the material in a parallel plate capacitor. Figure 1.2 (a) and (b) shows a parallel plate capacitor without and with dielectric material, which is placed between two metal plates and separated by a distance respectively.

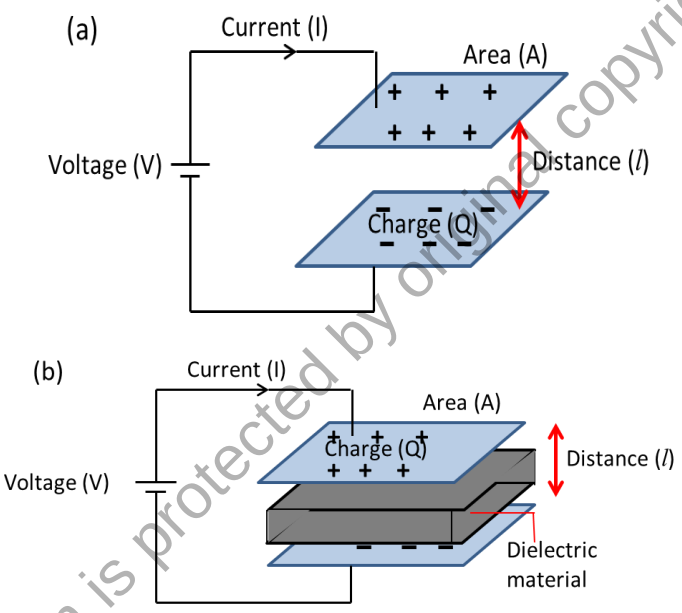

Figure 1.2: Parallel plate capacitor (a) without and (b) with dielectric material between the plates.

©This item is protected by original copyright

Figure 1.2(a) shows a simple parallel-plate capacitor in vacuum condition. In vacuum condition, there is only free space as a dielectric in between the parallel plates. When the voltage is applied, the positive charges and negative charges will be produced at each plate. The charge is found to be directly proportional to the applied voltage through the Equation 1.1 of:

$$C = Q/V \tag{1.1}$$

where C is the capacitance, Q is the charge and V is the applied voltage. By increasing the voltage more charge is accumulated at each plate and the capacitance value of capacitor will increase. The capacitance of a capacitor is a measure of its ability to store electric charge (Ekanath, 2012). The capacitance value of a capacitor with vacuum between the plates can be calculated using Equation 1.2 below;

$$C = \varepsilon_o \frac{A}{l} \tag{1.2}$$

where ε_o is dielectric constant of free space which is 8.854 x 10^{-12} F/m (Callister, 2001), A is the area of the plates in meters, l is distance between plates in meters and C is the capacitance in Farad. So, the capacitance will only depend on the geometric factor since the ε_o is constant. By increasing the area, the capacitance will be increased.

Figure 1.2(b) shows the parallel plate capacitor with the effect of the dielectric constant (ε_r) or known as permittivity. When a dielectric fills the space between the plates as shown in Figure 1.2(b), the capacitance will be increased by a factor of ε_r. Based on Figure 1.2 (b), the capacitance of two conducting plate can be calculated using the Equation 1.3.

$$C = \varepsilon_r \varepsilon_o \frac{A}{l} \tag{1.3}$$

© This item is protected by original copyright

where C is the capacitance in Farads, ε_r is the dielectric constant of material, ε_o is the dielectric constant of free space, A is the area of plate and *l* is distance between plates in meters. From the equation, in order to increase the capacitance, three parameters can be modified by increasing the area of metal plates, decreasing the distance between the plates and increasing the dielectric constant.

As the area of the metal plate increases, the capacitance value also increases as it is directly proportional to the capacitance. But this can be achieved only up to a small value. As we increase the area more and more, there is no more miniaturization and capacitor becomes more bulky and it would be difficult to include the capacitor in miniature level circuits. The distance between the plates is inversely proportional to the capacitance. Hence, decreasing the distance may seem to be a good idea to increase the capacitance. But as the distance between the plates decreases, the charges can be easily attracted towards each other thus creating an electrical short. Hence it no longer acts as a capacitor, but just a shorted wire. This is also termed as dielectric breakdown (A. J. Moulson & Herbert, 2003). Hence capacitors with very low distance of separation may have very low dielectric breakdown strength. Besides, increasing the dielectric constant has been a promising technique in increasing the capacitance of the capacitor. Hence, the research is focused in increasing the capacitance by increasing the dielectric constant. Increasing the dielectric constant value will not degrade the performance of the capacitor. Thus, choosing a dielectric with high dielectric constant value would be a good approach.

©This item is protected by original copyright